BY-NC

Kamil Gądek, Lechosław Tuz

The Assessment of the Microstructure and Selected Mechanical Properties of Butt Joints in Ferritic-Austenitic Duplex Steel

Abstract: The paper presents results of microscopic tests as well as results of tests concerning mechanical properties of MAG (136) welded joints in duplex steel X2CrNiMoN22-5-3 (1.4462). The research involved metallographic tests of the base material, heat affected zone and weld metal as well as Vickers hardness tests, static tensile tests, bend tests and the identification of a ferrite content obtained using a ferritiscope. The results of observations involving the microstructure of the particular zones of the welded joint as well as the quantitative analysis of phases and the results of the tests concerning the mechanical properties of the joints enabled the formulation of conclusions regarding the microstructure and the mechanical properties of the test joints.

Keywords: duplex, ferritic-austenitic steel, stainless steel, chemical tankers, welded joint microstructure

DOI: *10.17729/ebis.2019.2/3*

Introduction

The second half of the 20th century saw the rapid development of ferritic-austenitic steels also referred to as duplex steels because of their two-phase structure. The popularity of these steels results from their high corrosion resistance in environments characterised by the presence of chemical substances aggressively affecting the container material. Another factor responsible for the growing popularity of duplex steels is the decreased content of nickel, reducing the price of duplex steels to the level comparable with prices of austenitic steels [1]. Duplex steels are used in structures and industrial systems used in aggressive corrosive environments, e.g. in seawater desalination system elements, machinery parts used in the pulp and paper-making industry (e.g. rotors or shafts) characterised by high resistance to corrosion fatigue. Industrial sectors where duplex steels have found particularly extensive applications are the chemical and petrochemical industries. Duplex steels are used in the production of storage tanks and pipelines transporting crude oil and various acids [1-4] as well as when making tanks of chemical cargo carriers used in the sea transport of acids, crude oil refinement products and food industry products including animals fats, vegetable oils, wine or molasses [1, 5, 6]. An indispensable process of the production of large-sized structures made of duplex steels is welding. The welding thermal cycle and

mgr inż. Kamil Gądek (MSc Eng.); dr inż. Lechosław Tuz (PhD (DSc) Eng., (IWE, IWI)) – AGH University of Science and Technology in Kraków; Department of Physical and Powder Metallurgy

BY-NC

precipitation processes are responsible for the fact that the obtainment of appropriate properties of duplex steels is frequently difficult, thus significantly affecting the properties of a fabricated structure in terms of its corrosion resistance and mechanical properties [1, 7].

During welding processes, the welding thermal cycle accompanying the making of subsequent runs triggers δ→γ and γ→δ transformations in the weld and heat affected zone (HAZ). The foregoing is responsible for the occurrence of an unfavourable phenomenon of ferritisation in the HAZ, reducing the content of austenite and deteriorating both the plastic properties and the corrosion resistance of the joint. Other unfavourable phenomena include the grain growth and precipitation processes, taking place both in the weld and in the HAZ, leading to the formation of numerous intermetallic phases, carbides, nitrides or secondary austenite. Because of the above-named factors, the welding of duplex steels often requires the observance of related recommendations concerning the selection of filler metals as well as the use of appropriate linear energy and interpass temperature [7-12].

Testing methodology

Tests involved a butt joint made in one of the Polish shipyards making ocean-going ships transporting corrosion aggressive substances with containers made of duplex steel. The geometric characteristic of weld groove preparation is presented in Figure 1.

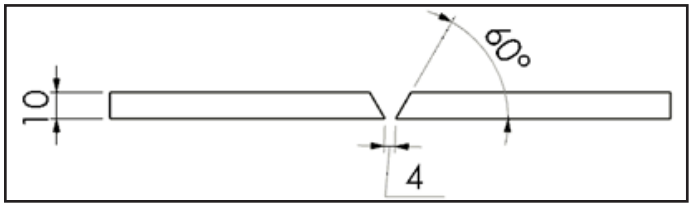

Fig. 1. Geometry and dimensions of the test joint weld groove

The MAG welded joint was made using a flux-cored filler metal wire in the vertical up position (PF). The shielding gas used in the process was a mixture of Ar (80%) and CO_2 (20%) in accordance with ISO 14175-M21. The root of the weld was formed using a ceramic backing strip. The joint was made of steel X2CrNiMoN22-5-3 (1.4462) using the Cromacore DW 329AP flux-cored filler metal designated as ISO 17633-A: T 22 9 3 N L P M/C 1. The chemical compositions of the steel and of the filler metal wire (in accordance with related standards) are presented in Table 1 and Table 2. The consistence of the chemical composition of the steel with the normalised chemical composition was verified using a spark emission spectrometer. The test result confirmed the appropriate contents of alloying elements. The consistence of the chemical composition of the flux-cored filler metal wire with the normalised chemical composition was ascertained on the basis of inspection certificate 3.1.

Table 1. Chemical composition (heat analysis) of steel 1.4462 in accordance with PN-EN ISO 10088-1 (% by weight) and selected mechanical properties in accordance with PN-EN 10088-4.

C max	Si	Mn	P max	S max	Ni	N	Cr	Mo	Cu	W
0.03	≤ 1.00	≤ 2.00	0.035	0.015	4.5-6.5	0.1-0.22	21.0-23.0	2.5-3.5	-	-
$R_{p0.2}$ min.				R_m			A – Elongation at rupture min.			
460 MPa				640-840 MPa			25 %			

Table 2. Chemical composition of the Cromacore DW 329AP flux-cored filler metal wire in accordance with ISO 17633 (% by weight)

C max	Si	Mn	P max	S max	Ni	N	Cr	Mo	Cu
0.04	≤ 1.2	≤ 2.5	0.03	0.025	7.5-10.5	0.08-0.2	21-24	2.5-4	<0.5

BY-NC

The research-related tests included the visual tests (VT) and the radiographic tests (RT) of the butt joint. The above-named tests were followed by the metallographic observations involving light microscopy and mechanical tests including Vickers hardness tests, uniaxial static tensile tests and bend tests. The magnetic phase content in the weld area, in the area adjacent to the weld and in the base material outside the effect of welding process heat was determined using a ferritiscope.

Test results

Visual and radiographic tests

The first stage of tests involved the visual tests (VT) of the joint, the face and root of which are presented in Figure 2. The face and the root were characterised by regular scaliness. The proper shape of the root was undoubtedly ensured by the use of a ceramic backing strip. Neither the face side nor the root side contained undercuts. The observation of the weld led to the conclusion that the joint represented quality level B in accordance with PN-EN ISO 5817.

The visual tests were followed by radiographic tests aimed to detect internal welding imperfections (if any). The radiogram (Fig. 3) presents a bright core with darker areas, resulting from difference of X-radiation absorption related to the scaliness responsible for differences of excess weld metal height. The radiogram did not reveal the presence of any welding imperfections.

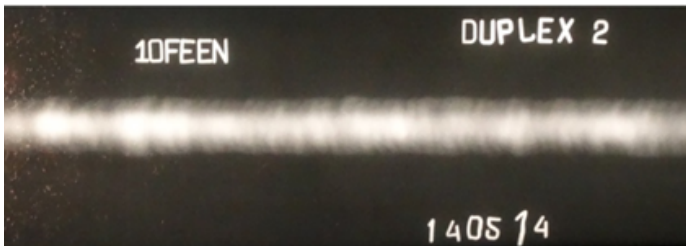

Fig. 3. Radiogram of the test joint

Metallographic tests

Metallographic tests involving a specimen etched in CrO_3 and NaOH were performed using a light microscope. The first area subjected to microscopic observations was the base material (MR). The photographs revealed a two-phase microstructure composed of austenite grains (γ) located in the matrix consisting of ferrite (δ) (Fig. 4). The two-phase microstructure was characterised by both grain shape and size-related heterogeneity dominated by the banded structure, where austenite grains were elongated in parallel to the rolling surface.

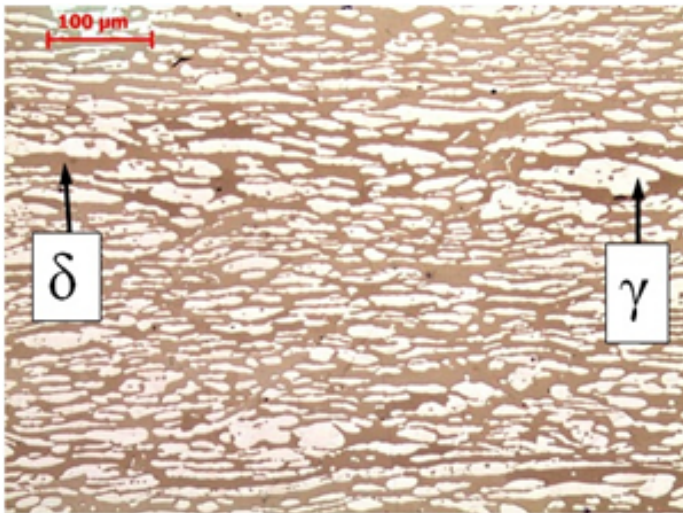

Fig. 4. Microstructure of the base material of steel X2CrNiMoN22-5-3

Along with the decreasing distance to the heat affected zone (HAZ), the elongated austenite bands disappeared and the morphology of the interphase boundary changed (Fig. 5). Figure 5b presents the boundary of ferrite grains.

Fig. 2. Welded joint: a) weld root and b) weld face

BY-NC

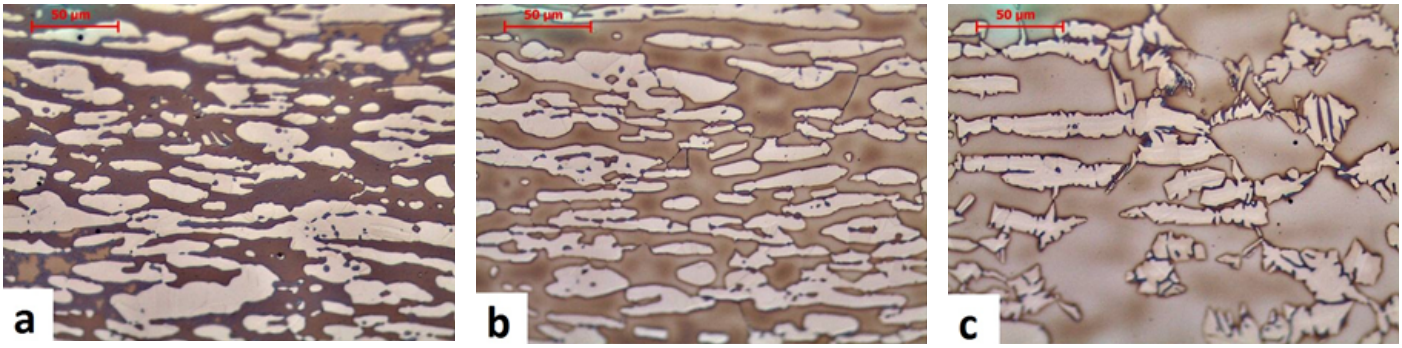

Fig. 5. Microstructure of a-b) base material, c) BM/HAZ boundary area

The heat affected zone revealed an increase in the content of ferrite, which was ascertained on the basis of the analysis of microstructural images subjected to decimal-to-binary conversion performed using the ImageJ software programme (Fig. 6). The ferrite content in the structure of the welded steel amounted to 49% (Fig. 5a) and grew along with a decreasing distance to the HAZ, reaching 62% (Fig. 5c).

Fig. 6. Photographs 5a and 5c subjected to decimal-to-binary conversion aimed to identify the percentage contents of structural constituents; ferrite – white areas, austenite – black areas

The heat affected zone (HAZ) was a coarse-grained area characterised by the greater amount of ferrite if compared with that of the base material (Fig. 7). The weld area revealed boundaries of crystallites growing perpendicularly from the fusion line, which was connected with the presence of the dendritic structure characteristic of the material in the as-cast state.

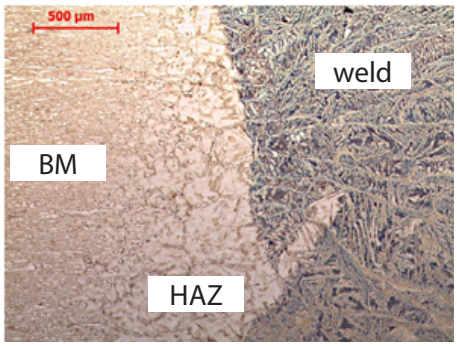

Fig. 7. Joint microstructure at the boundary between the root run and the second run

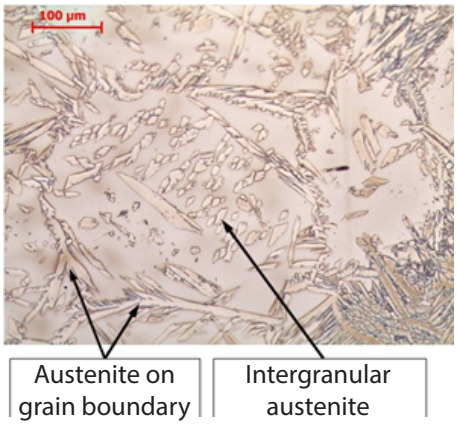

Fig. 8. HAZ microstructure

The HAZ area revealed the presence of austenite growing from grain boundaries and located within them. In the metallographic specimen plane, austenite had the shape of lamellas, whereas within grains it had the shape of parallelograms (Fig. 8). The aforesaid shape resulted from the mechanism through which austenite was formed from ferrite, which during cooling usually transforms in accordance with the Kurdjumov-Sachs relationship.

Parallelepiped grains of austenite can be formed as a result of the heterogenic nucleation of austenite within grains of ferrite. Alternatively, the above-named grains can be cross-cuts of austenite lamellas growing from the boundary of grains located below the metallographic specimen surface. At the boundary between the root run and the second run, the HAZ width amounted to approximately 800 µm. The content of ferrite in the HAZ structure was restricted within the range of 68% to 70%.

The HAZ in the root run area contained fine-dispersive precipitates located in the central part of the austenite grains as well as on the

BY-NC

boundary of ferrite and intergranular austenite (Fig. 9a). The HAZ did not reveal the presence of precipitates accompanying the making of the last run (Fig. 9b).

Figures 10a and b present a "tongue-like" area formed by the "pulling" of the base material to the weld when making a successive run, resulting from the application of the weave bead technique. The weld structure contained acicular-lamellar austenite (Fig. 10a). The bottom part of the "tongue" contained Widmastätten-structured lamellas, nucleating from austenite on the boundary of crystallite (Fig. 10b).

The content of ferrite in the weld structure was restricted within the range of 25% to 35%. The weld was characterised by the austenitic-ferritic microstructure and a significant austenite content (Fig. 11a,b), which resulted from the use of the filler metal characterised by the greater content of nickel in comparison with that of the base material. The root run area near the fusion line between runs revealed slight ferritic precipitates in austenite (Fig. 11b).

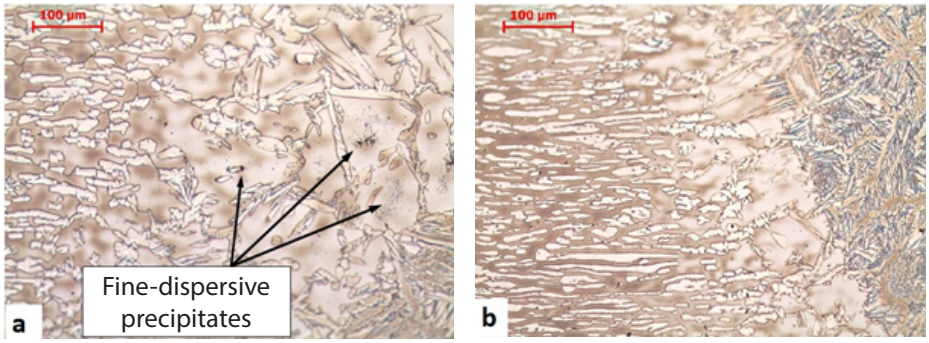

Fig. 9. HAZ microstructure at the root run and at the last run

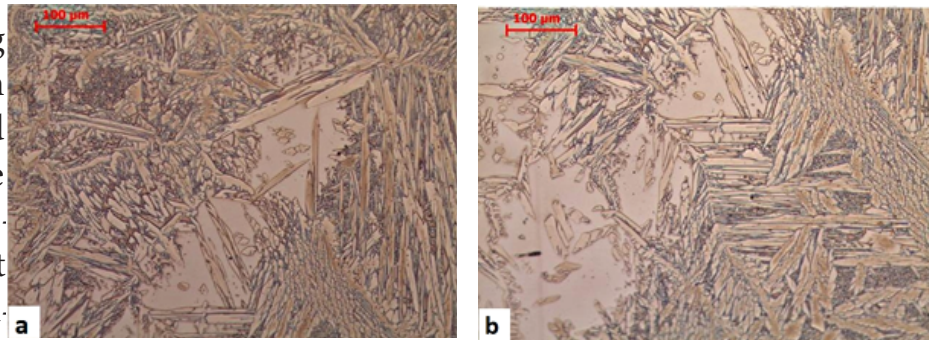

Fig. 10. Microstructure in the "tongue" area

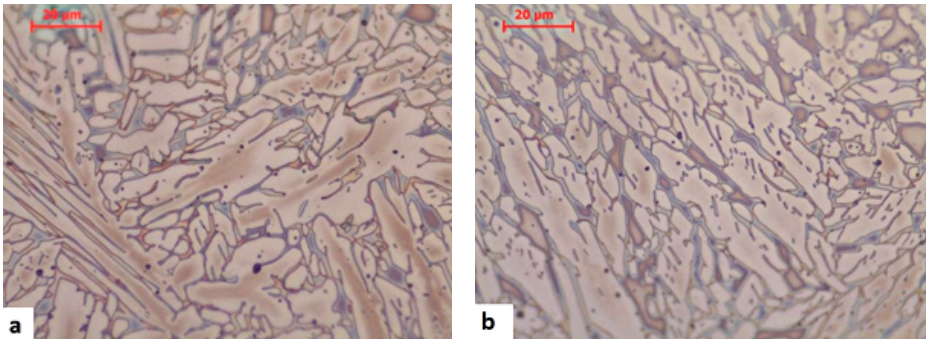

Fig. 11. Weld microstructure

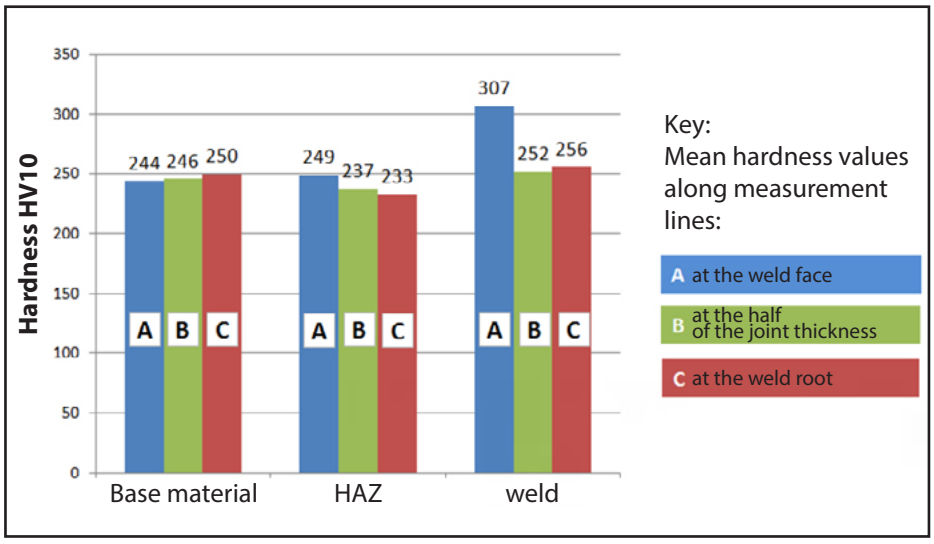

Fig. 12. Hardness distribution in the test joint

Hardness measurements

The first stage of mechanical tests involved the performance of Vickers hardness test under a load of 10 kG (HV10). The measurements were performed along three measurement lines, i.e. at the weld root, at the weld face and at the half of the joint thickness. The measured values obtained at the weld root and at the half of the joint thickness did not reveal any significant differences. In turn, the weld face revealed an increase in hardness by 55 HV10 in comparison

BY-NC

with the area located at the half of the joint thickness (Fig. 12).

Uniaxial static tensile test

The specimen was then subjected to a uniaxial tensile test performed perpendicularly in relation to the welded joint axis. The specimen ruptured in the base material, which enabled the determination of both the tensile strength and the conventional yield point (identified on the basis of a related stress-strain curve – see Fig. 13).

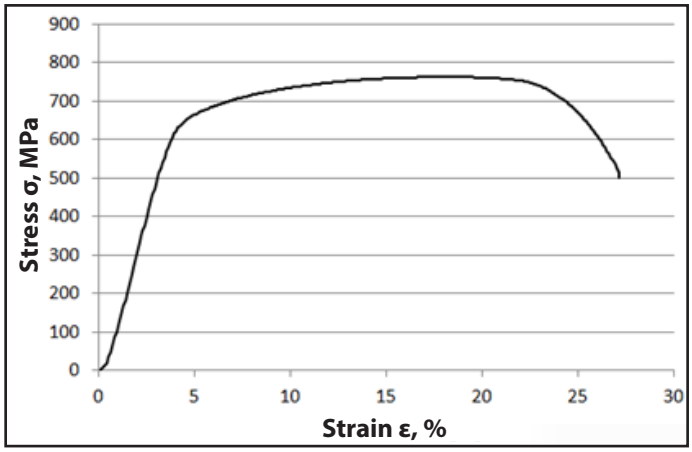

Fig. 13. Stress-strain curve of the welded joint

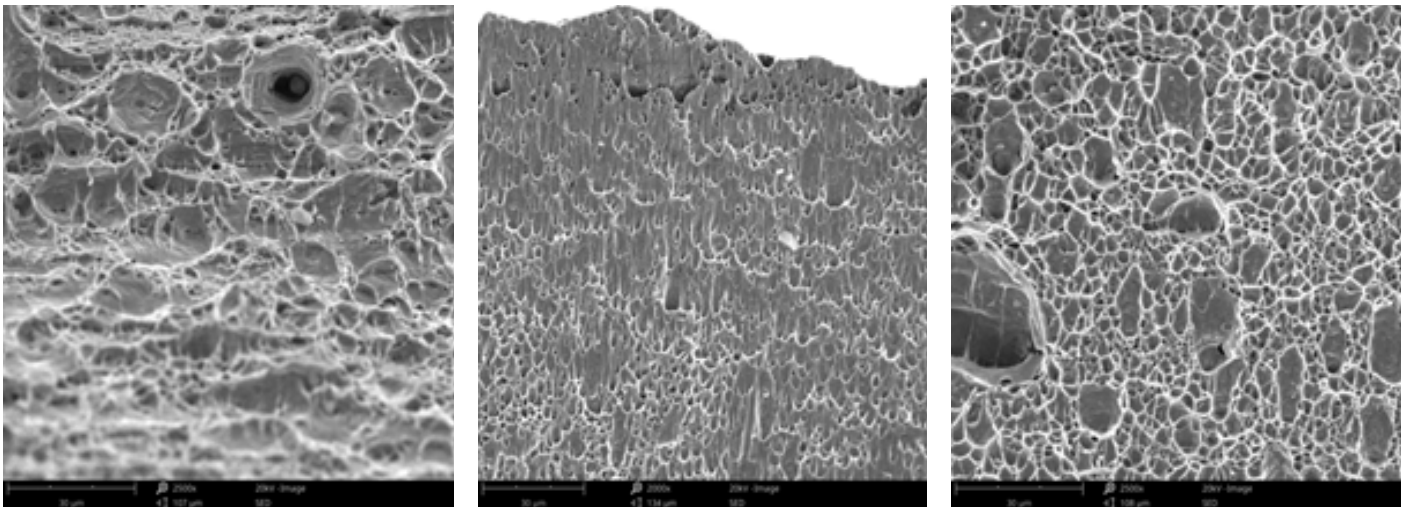

Fig. 14. Fracture topography

The tensile strength (Rm) determined on data obtained in the test amounted to 736 MPa, whereas the conventional yield point (Rpo,2) amounted to 545 MPa and was restricted within a related range specified in the PN-EN ISO 10088-4 standard.

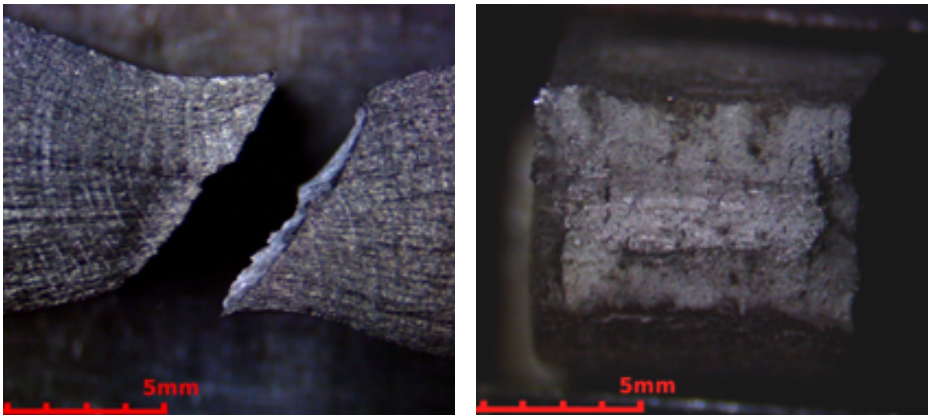

Fig. 15. Macroscopic photographs of the specimen fracture

Fractographic tests performed using scanning electron microscopy revealed the ductile nature of the fracture (Fig. 14). During the tensile test, the specimen necked down. The angle of the fracture plane in relation to the specimen plane amounted to approximately 50°, which confirmed the high plasticity of the material (Fig. 15).

Side bend test

The final stage of the tests identifying the mechanical properties of the joint included the performance of bend tests involving two specimens. In both cases, the specimen did not reveal any cracks on the surface. The maximum bend force recorded during the test amounted to 5.9 kN in relation to specimen no. 1 and

BY-NC

5.1 kN in relation to specimen no. 2. The specimen after the bend test is presented in Figure 16.

Fig. 16. Specimen after the bend test

Magnetic phase measurements

To identify the magnetic phase content, the test joint was subjected to ferritiscope-based measurements (performed both on the face and root side). Figure 17 presents test results.

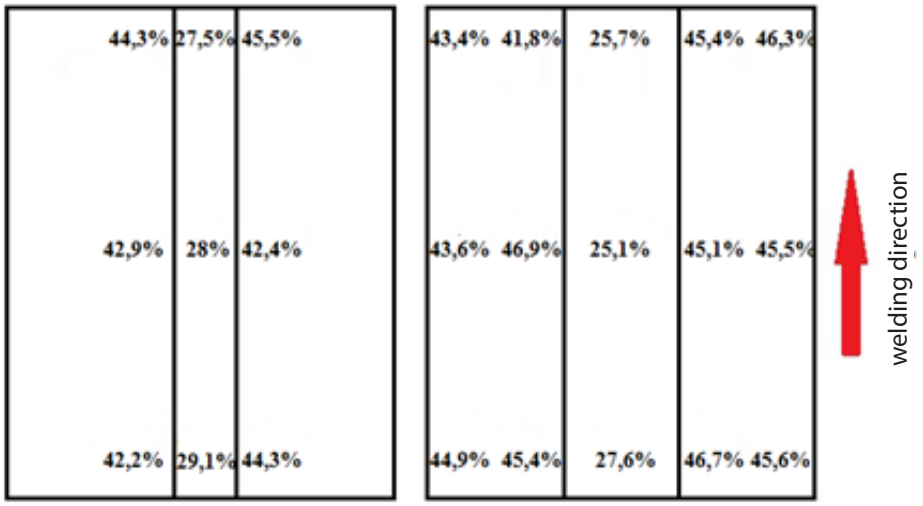

Fig. 17. Magnetic phase content measurement results

The obtained values were restricted within the range of 25% to 75% (defined as proper). The lower limit of the range corresponds to appropriate stress corrosion resistance, whereas the upper limit corresponds to appropriate plastic properties of the joint [7]. As regards the magnetic phase content, the tests revealed a significant difference between the weld and the remaining areas of the joint (resulting for the application of the filler metal characterised by a greater content of austenite-forming elements). The difference between the ferrite content-related test results obtained after the analysis of microstructural images and those obtained using the ferritiscope was the consequence of the sheet surface roughness as well as the face and root convexity [13].

Summary

The tests involved the assessment of the microstructure and selected mechanical properties of the arc welded joint made of ferritic-austenitic (duplex type) steel. The visual tests (VT) revealed that the joint represented quality level B in accordance with PN-EN ISO 5817:2014. The radiogram did not reveal the presence of welding imperfections. The results of the metallographic tests and of the tests concerning selected mechanical properties justified the formulation of the following conclusions:

1. The weld contained the fine-crystalline austenitic-ferritic structure characterised by the significant content of austenite.
2. The austenite-ferrite ratio in individual zones of the joint identified on the basis of microstructural photographs and measurements performed using the ferritiscope was restricted within the range regarded as proper and providing appropriate properties of the joint.
3. The narrow heat affected zone was coarse-grained, which resulted from grain growth and ferritisation processes, characteristic of duplex steel welding. The detection of the presence of fine-dispersive precipitates located in the central ferrite grain areas as well

BY-NC

as on the boundary of ferrite and intergranular austenite necessitated the performance of joint corrosion resistance tests and impact strength tests.

4. The three-point bend test did not reveal the presence of cracks on the surface of the specimens, which indicated the high plastic properties of the test joint. In the static uniaxial tensile test, the specimen ruptured in the base material. The ductile nature of the fracture ascertained on the basis of the fractographic tests indicated the appropriate amount of austenite in the welded steel.

References:

[1] Nowacki J.: Stal dupleks w konstrukcjach spawanych. Wydawnictwo WNT, Warszawa 2013.

[2] Brytan Z.: Stal duplex - rozwój mikrostruktury, własności mechaniczne, odporność korozyjna. Materiały z międzynarodowych targów METAL-FORUM 2010. [online], data dostępu: 18. 07. 2018, http://www.stalenierdzewne.pl/upload/file/publikacje/Stal_duplex_-_rozwoj_mikrostruktury_wlasnosci_mechaniczne_odpornosc_korozyjna.pdf.

[3] Willför M.: Stale duplex - Grupa wysokowytrzymałych gatunków stali nierdzewnej. Materials of the seminar: Zastosowanie stali odpornych na korozję. Trendy, kierunki, rozwój, 2008. [online], data dostępu 18.07.2018, http://www.stalenierdzewne.pl/upload/file/publikacje/1_Mikael_Willfor.pdf.

[4] Potapczyk A., Bielanik J.: Zastosowanie technologii lutowania próżniowego w procesie wytwarzania elementów maszyn ze stali duplex. Przegląd Spawalnictwa, 2007, no. 9, pp. 89-94.

[5] Neessen F., Bandsma P.: Użycie nierdzewnych stali DUPLEX do budowy zbiornikowców. Biuletyn Instytutu Spawalnictwa, 2002, no. 4, pp. 61-63.

[6] Słodziński S., Zając P.: Spawanie stali duplex w Stoczni Szczecińskiej Nowa S.A. Przegląd Spawalnictwa, 2003, no. 9-10, pp. 21-23.

[7] Tasak E., Ziewiec A.: Spawalność materiałów konstrukcyjnych. Tom 1. Spawalność stali. Wydawnictwo JAK, Kraków 2009.

[8] Karlsson L.: Spawanie stali odpornych na korozję - Stale duplex i superduplex. Biuletyn Instytutu Spawalnictwa, 1999, no. 1, pp. 28-33.

[9] Nowacki J.: Materiałowo-technologiczne aspekty spawania stali duplex w przemyśle okrętowym. Inżynieria Materiałowa, 2003, no. 6, pp. 746-750.

[10] Łukojć A., Nowacki J.: Wpływ warunków cieplnych spawania na strukturę i własności strefy wpływu ciepła połączeń stali duplex. Inżynieria Materiałowa, 2004, no. 6, pp. 734-737.

[11] Ammann T.: Spawanie stali typu duplex w osłonie gazów ochronnych. Biuletyn Instytutu Spawalnictwa, 2000, no. 5, pp. 69-74.

[12] Jakubowski J., Senkara J.: Zgrzewanie rezystancyjne punktowe austenityczno-ferrytycznej nierdzewnej stali duplex 2205. Przegląd Spawalnictwa, 2007, no. 8, pp. 79-82.

[13] Niagaj J., Mazur Ł.: Pomiar ferrytu w stali lean duplex S32101 i jej złączach spawanych. Biuletyn Instytutu Spawalnictwa, 2011, no. 1, pp. 45-52.